Nanoscale

PAPER

View Article Online
View Journal | View Issue

Cite this: *Nanoscale*, 2024, **16**, 10637

Superhydrophobic MOF/polymer composite with hierarchical porosity for boosting catalytic performance in an humid environment†

Ming-Liang Gao, ‡[a,b] Shuo Liu,‡[a] Lin Liu *[a] and Zheng-Bo Han *[a]

Received 5th March 2024,
Accepted 30th April 2024

DOI: 10.1039/d4nr00948g

rsc.li/nanoscale

The poor hydrostability of most reported metal–organic frameworks (MOFs) has become a daunting challenge in their practical applications. Recently, MOFs combined with multifunctional polymers can act as a functional platform and exhibit unique catalytic performance; they can not only inherit the outstanding properties of the two components but also offer unique synergistic effects. Herein, an original porous polymer-confined strategy has been developed to prepare a superhydrophobic MOF composite to significantly enhance its moisture or water resistance. The selective nucleation and growth of MOF nanocrystals confined in the pore of PDVB-vim are closely related to the structure-directing and coordination-modulating properties of PDVB-vim. The resultant MOF/PDVB-vim composite not only produces superior superhydrophobicity without significantly disturbing the original features but also exhibits a novel catalytic activity in the Friedel–Crafts alkylation reaction of indoles with *trans*-β-nitrostyrene because of the accessible sites and synergistic effects.

1. Introduction

Heterogeneous catalysts applied in many areas of chemical and pharmaceutical industries have numerous advantages such as the ease of recovery, reusability and stability.[1] Most often, water molecules, a typical byproduct originating from a humid environment, can co-adsorb or coordinate with active sites on hydrophilic heterogeneous acidic catalysts and are one of the negative components for acid-catalyzed reactions.[2] This can cause partial deactivation of the acidic sites, thus restraining the chemical reaction process and efficiency.[3] Moreover, in some cases, many heterogeneous Lewis acid catalysts are unstable in moisture systems and tend to hydrolyze.[3,4] These disadvantages severely limit the performance of this kind of catalyst in some practical applications. Consequently, the fabrication of hydrophobic, especially superhydrophobic catalysts that keep water molecules away from catalytic sites and reactants, is a promising method for resolving these problems.[5] Furthermore, regulating the microenvironment of heterogeneous catalytic systems from hydrophilicity to hydrophobicity could promote the adsorption capacity of catalysts for oleophilic reactants, which will further enhance the catalytic activity in many organic transformation reactions.[6]

Metal–organic frameworks (MOFs), constructed using adjustable metal ions or metal clusters as nodes and organic ligands as linkers, have become a well-known class of porous crystalline materials.[7] Because of their nanoscale periodicity, permanent porosity, channel functionalization, and structural diversity, MOFs can be rationally designed and prepared to afford versatile desired applications, such as heterogeneous catalysis,[8] gas storage and separation,[9,10] Researchers have explored varied approaches to improve the catalytic performance of MOFs by controlling their microenvironment.[11] However, a great deal of MOFs with weak coordination bonds can be easily destroyed under a humid environment, which has been recognized as the major encumbrance limiting their practical application.[11a] Accordingly, rapid and promising progress has been witnessed in fabricating hydrophobic MOFs to overcome their inherent weaknesses and endow them with improved or novel functionalities for diverse applications.[12] To date, two common approaches have been adopted to construct hydrophobic MOFs: one approach is concerned with fabricating a rough surface or external surface corrugation with an anisotropic crystal morphology; the other approach is mainly focused on lowering the surface free energy, which is to introduce hydrophobic moieties in MOFs through post-synthetic modification.[13] Although the stability of MOFs under moisture conditions can be improved, these approaches have disadvan-

[a]*College of Chemistry, Liaoning University, Shenyang 110036, P. R. China. E-mail: ceshzb@lnu.edu.cn, liulin@lnu.edu.cn*
[b]*Department of Chemistry, University of Science and Technology of China, Hefei, Anhui 230026, P. R. China*

†Electronic supplementary information (ESI) available. See DOI: https://doi.org/10.1039/d4nr00948g

‡These authors contributed equally to this work.

tages and limitations, such as tedious procedures, complex instrumentation, and reduced porosity.[14] The points mentioned above motivated us to design and engineer MOF-based composites with admirable hydrophobic/superhydrophobic features, large specific surface area, and superior catalytic properties.

Herein, we report a facile strategy that can prepare superhydrophobic nanocomposite with hierarchical porosity by directly growing microporous ZIF-8 nanocrystals within the superhydrophobic porous polymer (PDVB-vim) to form the ZIF-8/PDVB-vim composite. Thus-obtained composite possesses preeminent superhydrophobicity, high void fractions, and excellent stability. In contrast to the ZIF-8 counterpart and other known MOF-based catalysts, the resulting superhydrophobic ZIF-8/PDVB-vim composite exhibited remarkably higher catalytic activity and recyclability for the Friedel–Crafts alkylation reaction of indoles with *trans*-β-nitrostyrene under air atmosphere at a mild temperature. To the best of our knowledge, this is the first example of superhydrophobic MOF composite catalyst prepared by a porous polymer-confined strategy.

2. Results and discussion

2.1. Fabrication and characterization of ZIF-8/PDVB-vim catalysts

ZIF-8/PDVB-vim composite was prepared through a facile strategy for confining ZIF-8 nanoparticles into a superhydrophobic porous PDVB-vim support material (Fig. 1a). The selectively controlled nucleation and growth of ZIF-8 nanocrystals confined within the porous PDVB-vim occurred during the synthesis of liquid-phase nano-ZIF-8. The PXRD patterns of the

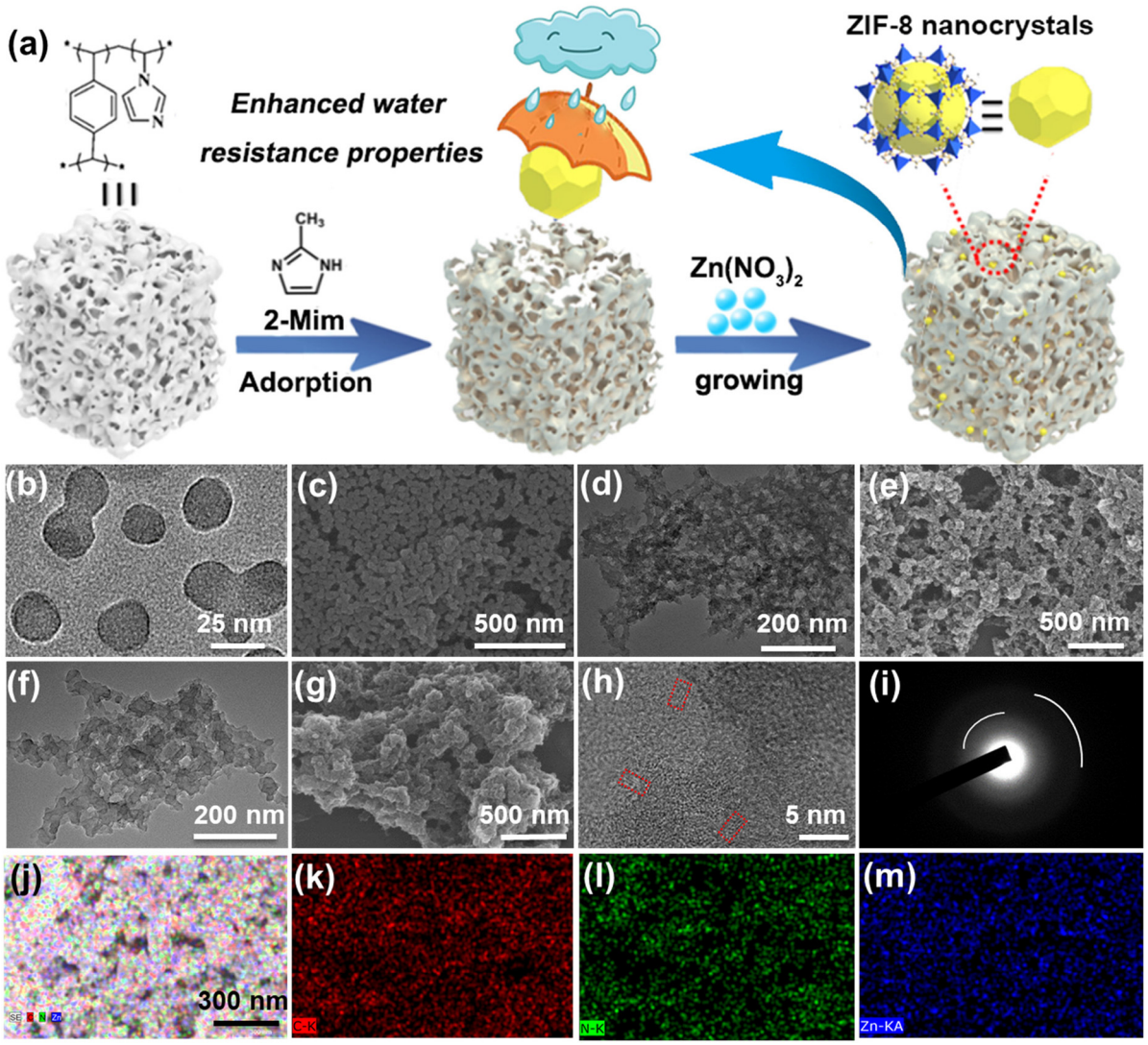

Fig. 1 (a) The synthetic route of the ZIF-8/PDVB-vim composite; TEM and SEM images of (b and c) ZIF-8; (d and e) PDVB-vim; (f and g) ZIF-8/PDVB-vim composite; (h and i) HRTEM image and selected-area electron diffraction (SAED) pattern of the ZIF-8/PDVB-vim composite; elemental mapping images of the ZIF-8/PDVB-vim sample (j–m).

as-prepared samples are shown in Fig. S1a† and show well-defined diffraction peaks. For PDVB-vim, there is a broad peak at about 18°, which is caused by its amorphous status. After incorporating ZIF-8 crystals into the inner pores of PDVB-vim, the pattern has the characteristics of both ZIF-8 and PDVB-vim and the intensity of the peaks is low in the composite. This indicates that a small-sized ZIF-8 crystal was successfully formed in the pores of PDVB-vim; FT-IR and Raman spectra were further used to investigate the possible components of the composite (Fig. S1b and c†). The characteristic absorption bands of pure ZIF-8 at 1175 and 1147 cm^{-1} in FT-IR spectra can be assigned to the C–C bond between imidazole and $–CH_3$ groups.[15] The absorption bands of PDVB-vim at 1605 and 1509 cm^{-1} can be assigned to stretching vibrations of the –C═C– bond.[16] In the Raman spectra, as can be observed, the bands at 284 cm^{-1}, 1149 cm^{-1}, and 1461 cm^{-1} are assigned to Zn–N stretching, C–N stretching of the imidazole ring, and methyl bending, respectively.[17] The strong bands were observed at 1609 and 1635 cm^{-1} corresponding to the –C═C– of the benzene ring in PDVB-vim.[18] After the combination of ZIF-8 and PDVB-vim, FT-IR and Raman spectra revealed the existence of characteristic peaks associated with the stretching mode of aromatic and imidazole C–H, aromatic C═C, C–N and C–C bond between the imidazole and $–CH_3$ groups as well as Zn–N stretching of ZIF-8, which indicates the presence of ZIF-8 and PDVB-vim components in this composite.

The micro-morphologies of ZIF-8, PDVB-vim and ZIF-8/PDVB-vim composite were evaluated by using various microscopic techniques (Fig. 1b–g). TEM and SEM micrographs of ZIF-8 show nanocrystals with sizes of about 25 ± 5 nm (Fig. 1b and c). The hierarchical meso-macroporosity of PDVB-vim can be observed from the TEM and SEM images (Fig. 1d and e), which indicate that the porous structure of PDVB-vim displays wormhole-like and disordered characteristics. From the observation in the TEM images shown in Fig. 1f, the surface morphology of ZIF-8/PDVB-vim composite is somewhat similar to that of pristine PDVB-vim, while ZIF-8 nanocrystals are very well dispersed in PDVB-vim. Moreover, the obvious reduction of the open pores can be found in the SEM images of ZIF-8/PDVB-vim composites (Fig. 1g). These observations are consistent with the hypothesis that ZIF-8 nanocrystals are confined within the inner pores of PDVB-vim. HRTEM image in Fig. 1h shows that the interplanar distances of the selected area are calculated to be ~0.49 nm, attributable to the (2 2 2) lattice planes of ZIF-8. The diffuse diffraction rings of the SAED pattern are typical characteristics of nanometric size particles, which can also confirm that the crystalline ZIF-8 consists of the porous composite (Fig. 1i). The *d* spacing of the (0 1 1) plane calculated from the SAED patterns is ~11.98 Å, in agreement with the value obtained from the PXRD pattern as well as reported values of the *d* spacing for crystalline ZIF-8 particles.[19] Importantly, the ZIF-8 nanoparticles are highly dispersed in the ZIF-8/PDVB-vim composite, which can be verified from the uniform distribution of the mapping of the corresponding elements detected by the EDS mapping (Fig. 1j–m).

To further explore the textural properties of ZIF-8/PDVB-vim composite, N_2 adsorption–desorption isotherms and pore size distribution measurements were determined. As shown in Fig. S2,† the isotherms of ZIF-8 are identified as type I, which is characteristic of microporous materials, while PDVB-vim and ZIF-8/PDVB-vim show type IV with an H4 hysteresis loop, which is the typical characteristic of the micro-mesopore structure. The BET-specific surface areas of ZIF-8, PDVB-vim and ZIF-8/PDVB-vim composite were 1296.7, 799.8 and 833.1 $m^2 g^{-1}$, respectively. Also, the pore size distributions for ZIF-8, PDVB-vim and ZIF-8/PDVB-vim composite were calculated using NLDFT models. From the observation of the pore size distribution shown in Fig. S3,† porous PDVB-vim with a pore diameter of about 0.5–64 nm is an ideal support for ZIF-8 nanocrystals. It is worth noting that the pore size ranging from 27.5 to 64.0 nm reduced obviously after the process of the preparation of the ZIF-8/PDVB-vim composite. At the same time, a significant increase of the pore from 0.5 to 1.0 nm can be observed. The results of the pore size distribution calculated from the N_2 adsorption isotherms at 77 K are consistent with SEM and TEM images. Based on these observations, it is concluded that porous PDVB-vim can act as a functional support (structure-directing) material for the selectively controlled nucleation and growth of nanoscale ZIF-8.

TG analysis under the N_2 atmosphere reveals that PDVB-vim, ZIF-8, and ZIF-8/PDVB-vim composite can be stabilized up to 350 °C, but with different residual weights at 750 °C (Fig. S4†). According to the results of TG analysis, the content of ZIF-8 in the ZIF-8/PDVB-vim composite was estimated to be 16.4%, in line with the ICP-OES test (Table S1,† entry 1). The chemical stability was tested by soaking the composite in MeOH, CH_2Cl_2, $CHCl_3$, toluene, and MeCN and adding nano CeO_2 as an internal standard for 24 h, the results of the coincident PXRD patterns verified that all the phase composition of ZIF-8/PDVB-vim composite are integrated (Fig. S5†). In addition, after being treated in an aqueous solution at 100 °C for 20 days, the PXRD tests reveal that the ZIF-8/PDVB-vim composite maintains the structural integrity of each component (Fig. S5†). The ZIF-8/PDVB-vim composite still retained good porosity after the boiling water treatment, which was verified by N_2 adsorption isotherms (Fig. S6†), demonstrating the excellent stability of the composite against degradation in the presence of water. ^1H NMR and ICP-OES tests of the ZIF-8/PDVB-vim composite after water treatment also confirmed the stability of the composite (Fig. S7 and Table S1,† entry 2). The pH durability tests on ZIF-8 and the PDVB-vim/ZIF-8 composite across a comprehensive pH range of 0–14 were further executed to assess their chemical stability. The results indicate that the PDVB-vim/ZIF-8 composite maintained stability across the entire pH range from 0 to 14, whereas ZIF-8 is only stable from pH 4 to 14 (Fig. S8†). These findings affirm that the polymer-confined strategy not only boosts hydrophobicity but also enhances pH durability. To investigate the effect of ZIF-8 confined in PDVB-vim, static water contact angle (SWCA) measurements were performed. As shown in Fig. 2a, ZIF-8 exhibited hydrophilicity and SWCA was ~84°. On the other

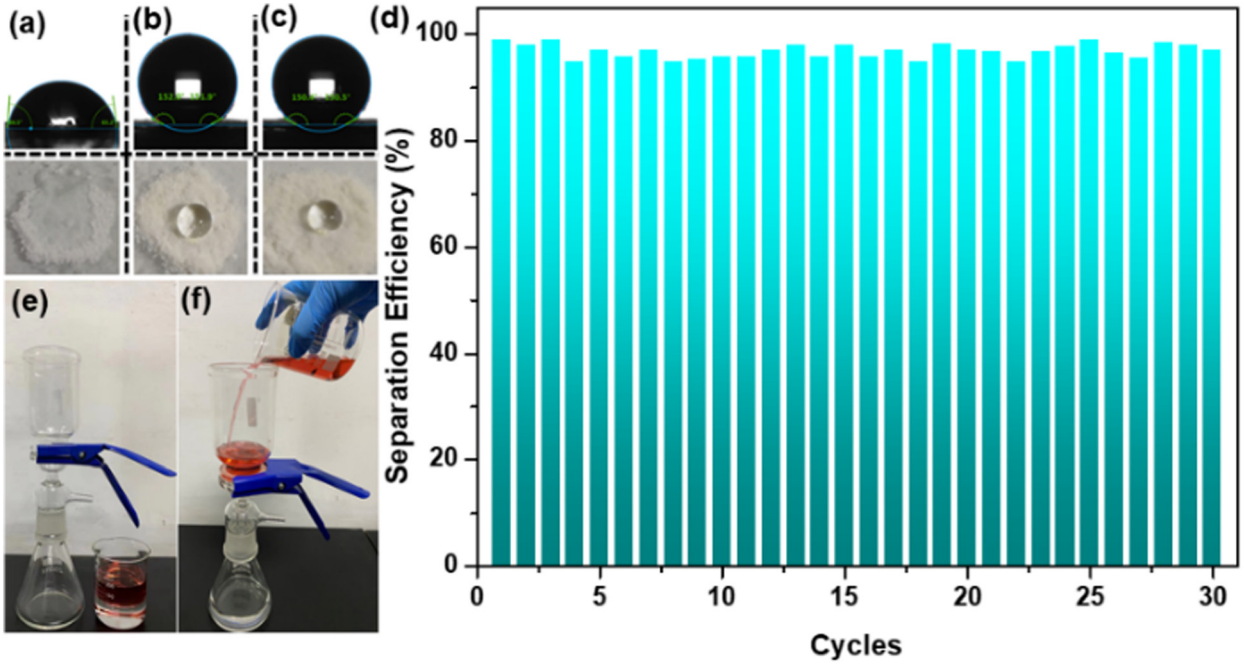

Fig. 2 The static water contact angle of ZIF-8 (a); PDVB-vim (b) and ZIF-8/PDVB-vim (c). Oil-water separation performance of PDVB-vim (d–f).

hand, the SWCA of water droplets on the ZIF-8/PDVB-vim composite showed contact angles up to ~150°. The transformation from hydrophilic to hydrophobic type can be attributed to the pristine superhydrophobic PDVB-vim with the SWCA is ~152° (Fig. 2b and c). In addition, the practical oil–water separation performance could be investigated to verify the superhydrophobic properties of this composite. According to previous reports, the separation device was generated by loading the ZIF-8/PDVB-vim composite on commercial filter paper.[20] Briefly, the $CHCl_3$–dyed water mixture was selected as an oil–water mixture model to test the separation performance under the force of gravity without any external force. The separation equipment images before and after the separation experiment are demonstrated in Fig. 2e and f. In the process of separation, $CHCl_3$ easily permeated through the filter paper, which was fixed between two glass devices, but the water was repelled and stayed in the upper part of the glass container, and the collected efficiency of $CHCl_3$ were all above 95% in 30 cycles. This result further demonstrates that the ZIF-8 nanocrystals are almost completely confined in PDVB-vim, which endows the composite with superior superhydrophobicity, thus forming a natural barrier protecting the MOF crystals. We are also convinced that this approach can be extended to many other MOF structures suffering from being water-labile. Therefore, it is expected that the superhydrophobic ZIF-8/PDVB-vim composite was successfully prepared on a large scale through a facile synthetic route, thus facilitating its practical application.

2.2 Catalysis studies

Many MOFs-based catalysts are prone to collapse after prolonged exposure to harsh reaction conditions, including in humid environments, demanding organic solvents, acid and alkali media.[21] Therefore, developing green MOFs-based catalysts that operate in a humid environment under mild conditions is critical and imminent. The successful strategy for the preparation of the above superhydrophobic and stable ZIF-8/PDVB-vim composite paves the way for the construction of superhydrophobic MOF-based catalysts by confining MOF nanocrystals into superhydrophobic porous polymers. In recent years, the conjugated addition of indoles to *trans*-β-nitrostyrene has been extensively studied, which provides an efficient strategy for synthesizing a variety of alkaloids.[22] The product of Friedel–Crafts alkylation of indoles with *trans*-β-nitrostyrene can be easily converted into melatonin derivatives, tetrahydro-β-carbolines and triptans, *etc.*[23]

To evaluate the catalytic activity of porous superhydrophobic ZIF-8/PDVB-vim composite under mild conditions, the liquid-phase Friedel–Crafts reaction of indole and *trans*-β-nitrostyrene was used as the model reaction to test the effect of hydrophobicity on the heterogeneous catalytic performance. To compare with previously reported MOF-based systems, we explored the catalytic activity of the ZIF-8/PDVB-vim composite in the Friedel–Crafts reaction at room temperature and analyzed the resulting products by ^1H NMR analysis (Fig. S9†). Before the catalytic experiments, all the catalysts were fully activated under a vacuum in sealed glassware to remove the guest molecules and provide accessible Lewis acid active sites for substrates. Firstly, the catalytic performance of ZIF-8 was assessed in the presence of MeCN at room temperature using a 5 mmol% catalyst based on the Lewis acid sites for 24 h under N_2 and air atmosphere (Table 1, entries 1–2, Fig. S10a and b†). In addition, the lower catalyst loading was used to distinguish the effect of water in air and N_2. The yield of the

Table 1 Optimization of reaction conditions for the Friedel–Crafts reaction

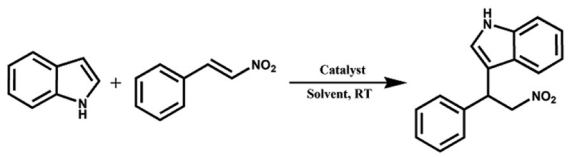

Entry	Cat.	Atmosphere	Sol.	Yield (%)
1	ZIF-8	N_2	MeCN	76.4
2	ZIF-8	Air	MeCN	44.4
3	ZIF-8/PDVB-vim	N_2	MeCN	>99
4	ZIF-8/PDVB-vim	Air	MeCN	>99
5	ZIF-8/PDVB-vim	Air	CH_2Cl_2	81.2
6	ZIF-8/PDVB-vim	Air	THF	53.0
7	ZIF-8/PDVB-vim	Air	MeOH	21.7
8	ZIF-8/PDVB-vim	Air	Toluene	76.4
9	No catalyst	Air	MeCN	Trace
10	PDVB-vim	Air	MeCN	5.6
11	$Zn(OAc)_2{\cdot}2H_2O$	Air	MeCN	38.3
12	2-Methylimidazole	Air	MeCN	Trace
13	ZIF-8 + PDVB-vim	Air	MeCN	78.9

trans-β-Nitrostyrene (150 mg, 1.0 mmol), indoles (180 mg, 1.5 mmol), catalyst 5 mol% based on Zn(II) center, MeCN 5 mL, under an N_2 or air atmosphere at 25 °C for 24 h. Determined by ^{1}H NMR.

product in ZIF-8/PDVB-vim was similar no matter whether air or N_2 was used. Yet, the results of ZIF-8 were distinguishing. It was found that the yield of the product depended on the atmosphere, N_2 atmosphere was better than the air atmosphere. As is well-known, the relative humidity of various air classifications is generally about 40% to 80%, and Lewis acid active sites are sensitive to moisture, which is a crucial factor in reducing the catalytic activity in organic reactions.[9–11] Hence, the phenomenon can be attributed to the water molecules from the humid air environment coordinated with the Zn centers to reduce the catalytic activity of ZIF-8. To confirm this hypothesis, a superhydrophobic porous ZIF-8/PDVB-vim composite was used as a catalyst under N_2 or air atmosphere in MeCN (Table 1, entries 3–4, Figs. S10c and d†). As expected, the yield of Friedel–Crafts reaction revealed gratifying performance improvement. The results described above make it clear that the superhydrophobic porous ZIF-8/PDVB-vim composite can resist the water molecules and also confirm that the formation of a superhydrophobic surface on the catalyst is effective in restraining the loss of catalytic activity. In the meantime, the solvent effect of the liquid-phase Friedel–Crafts reaction under air atmosphere was studied.

The yield of the product was found to be solvent-dependent when MeCN was chosen as the solvent, the yield was optimum (Table 1, entries 4–8, Fig. S10d–h†). According to the results of the solvent-dependent experiments, MeCN was selected as the solvent for the Friedel–Crafts reaction. It is also evident that under identical conditions, scarcely any product can be detected when no catalyst was added to the catalytic system (Table 1, entry 9). All the above data confirm that the catalyst is heterogeneous in nature and there is no leaching of active species into the solution. In addition, the catalytic activity was also compared with the component of ZIF-8/PDVB-vim, *i.e.*, PDVB-vim, $Zn(OAc)_2{\cdot}2H_2O$, and 2-Mim (Table 1, entries 10–12). There was a very low yield (5.6%) in the presence of PDVB-vim as a catalyst, which can be attributed to the lack of Lewis acid sites. With $Zn(OAc)_2{\cdot}2H_2O$, a yield of 38.3% was observed after 24 h and it is lower than the yield when ZIF-8 or ZIF-8/PDVB-vim act as a catalyst. This clearly shows the importance of the coordination effect of 2-Mim to the ZnII center promoting the increase in Lewis acid activity of the ZnII center donating environment more favorably. When using 2-Mim as the catalyst, traces of the target product were observed after the reaction. We further employed a mechanical mixture of ZIF-8 crystals and PDVB-vim to catalyze the reaction (Table 1, entry 13 and Fig. S11†). The results indicate that the catalytic performance of this physically mixed catalyst is inferior to that of the PDVB-vim/ZIF-8 composite. Besides, the yield *vs.* time and leaching experiments were performed for the reaction between indole and *trans*-β-nitrostyrene under the optimized reaction condition. As shown in Fig. S12,† the ZIF-8/PDVB-vim composite was filtered after 8 h and the resulting solution was allowed to continue until 24 h. Notably, the product formation was interrupted upon removal of the catalyst from the reaction mixture and it verifies that the presence of ZIF-8/PDVB-vim composite is very essential for the promotion of the Friedel–Crafts reaction.

Furthermore, the expansion of the substrate scope of Friedel–Crafts reactions with *trans*-β-nitrostyrene derivatives and various substituent indoles were explored using ZIF-8/PDVB-vim composite as a catalyst (summarized in Table 2, Fig. S13 and S14†). The results showed that both *trans*-β-nitrostyrene with electron-donating and electron-withdrawing groups could efficiently react with indole to form corresponding products in excellent yields of 96.9 and 100% (Table 2, entries 1 and 2). Next, the indole scope was examined by reacting *trans*-β-nitrostyrene with various indole compounds. The catalytic efficiency of the ZIF-8/PDVB-vim composite varied significantly for differently substituted indoles. 5-methyl-indole and 5-methoxy-indole as electron-rich substituted indole substrates were investigated and the yield of the respective products can reach 100% (Table 2, entries 3 and 4). This may be attributed to the indole ring facilitating activation by electron-donating methyl or methoxy groups through the way of nucleophilic attack. On the contrary, 5-chloro-indole as an electron-withdrawing group results in a yield of 84.1% with the corresponding product (Table 2, entry 5). More importantly, when *N*-methylindol was selected as substrate, the yield decreased dramatically to 20.6% (Table 2, entry 6). Furthermore, 2-methylindol and 2-phenylindole were used as the substituted substrate, analogously, the yields were 100% and 26.1%, respectively (Table 2, entries 7 and 8). This result can be used to prove the effectiveness of the steric factor for catalytic performance. On the whole, all the above results illustrate that the ZIF-8/PDVB-vim composite can efficiently catalyze the Friedel–Crafts reaction of the vast majority of substrates. The high yield may be ascribed to the strong adsorp-

Table 2 Substrate scope of *trans*-β-nitrostyrene derivatives and indole compounds in the Friedel–Crafts reaction

Entry	Substrate of indoles	Substrate of *trans*-β-nitrostyrene	Product	Yield (%)
1		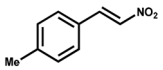	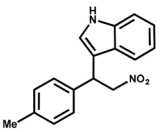	>99
2		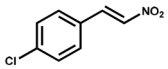	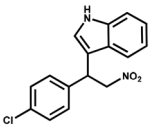	96.9
3	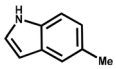	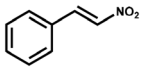	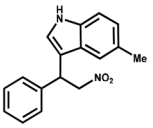	>99
4	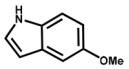	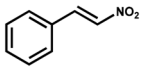	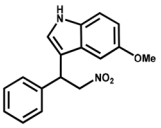	>99
5	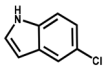	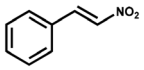	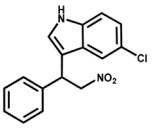	84.1
6		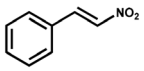	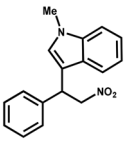	20.6
7	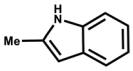	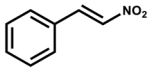	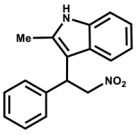	>99
8	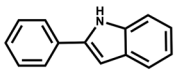	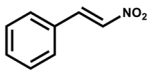	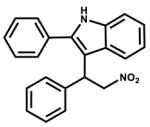	26.1

trans-β-Nitrostyrene derivatives (1.0 mmol), indoles (1.5 mmol), catalyst 5 mol% based on Zn(II) center, MeCN 5 mL at 25 °C for 24 h. Determined by ^{1}H NMR.

tion of the catalyst for reactants through positive hydrophobicity, intrinsic characteristics of porosity and H-bond interaction. In comparison to the reported MOF-based catalysts for Friedel–Crafts reaction of indoles and *trans*-β-nitrostyrene,[24] the efficiency of superhydrophobic ZIF-8/PDVB-vim is noteworthy (Table S3†).

Besides, excellent heterogeneous catalysts need to possess superior stability and reusability. On the basis of the above experimental results and assumptions, recycling experiments for the ZIF-8/PDVB-vim composite were performed and it clearly demonstrated no noticeable change in activity after 5 run recycle experiments (Fig. S15†). In addition, the FT-IR, Raman spectra PXRD patterns and ICP-OES of the recovered ZIF-8/PDVB-vim composite showed that the structure of the composite remained unchanged after the reaction, indicating that the composite had high stability and good recyclability under the catalytic conditions (Fig. S16–S18 and Table S1,† entry 3).

A proposed mechanism is presented involving the synergistic activation of the two reactants by ZIF-8/PDVB-vim composite for enhancing catalytic performances (Scheme 1). Firstly, Zn(II) centers as Lewis acidic sites in ZIF-8 can activate the nitro compound through the coordination interaction with the oxygen to increase the electrophilic character of the aliphatic carbon atom and is susceptible to the nucleophilic attack of indole. Secondly, the adjacent N atom in the ZIF-8 and PDVB-vim in this composite interacted with indole through a weak H-bonding effect, which can also gather and activate indole.[25] More interestingly, superhydrophobic ZIF-8/PDVB-vim composite can restrain the water molecules from the solvent or humid environment to influence the catalytic activity of ZIF-8. Thus, the formation of the alkylated product with higher yield

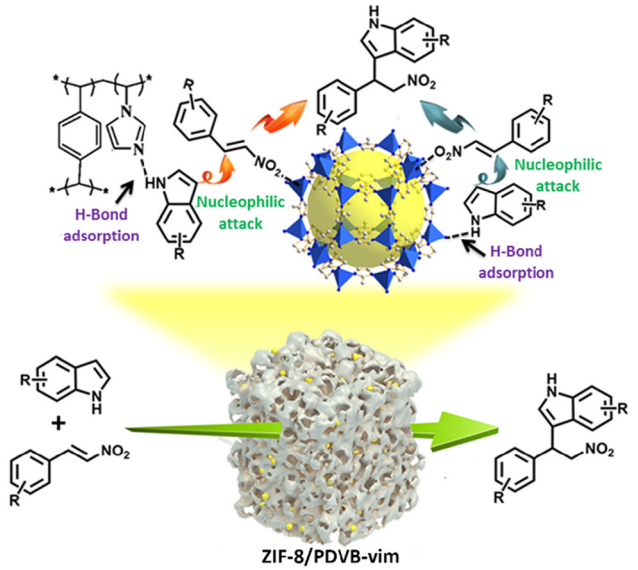

Scheme 1 The possible mechanism for the Friedel–Crafts reaction of indole with *trans*-β-nitrostyrene catalyzed by the ZIF-8/PDVB-vim composite.

is attributed to highly efficient and robust super-hydrophobic ZIF-8/PDVB-vim composite as catalyst-promoting reactions *via* the synergistic activation mechanism for two organic substrates. To support the mechanism, we studied the interaction of *trans*-β-nitrostyrene and indole with ZIF-8, PDVB-vim and the composite through UV-vis spectroscopy. A finely ground sample was used for facilitating close contact between the activity sites and *trans*-β-nitrostyreneo/indole in the adsorption experiments. As shown in Fig. S19,† the three samples show an obvious decrease in UV-vis spectroscopy upon successive addition of *trans*-β-nitrostyrene solution (λ = 311 nm) or indole solution (λ = 269 nm). The strong adsorption effect of the composite for *trans*-β-nitrostyrene solution and indole prove that the reactions are promoted *via* a synergistic activation mechanism for two organic substrates.

3. Conclusion

In summary, a porous polymer-confined strategy has been developed to prepare superhydrophobic nanocomposite with hierarchical porosity by directly growing MOF nanocrystals within the superhydrophobic porous polymer. As a result, the composite exhibits enhanced catalytic activity and improved reusability in Friedel–Crafts reaction under mild conditions due to a unique synergistic catalytic mechanism that relies on a synergy between Lewis acid active sites of ZIF-8 and H-bond activation in PDVB-vim. In a broader perspective, this novel strategy for preparing multifunctional superhydrophobic nanocomposites offered an opportunity for various practical applications including catalysis, oil–water separation, and electronic devices, *etc.*

Author contributions

The manuscript was written through contributions of all authors. All authors have given approval to the final version of the manuscript.

Conflicts of interest

There are no conflicts to declare.

Acknowledgements

The authors kindly acknowledge financial support from the National Natural Science Foundation of China (22171121 and 22101269), the Applied Basic Research Plan of Liaoning province (2023JH2/101300007), Liaoning Revitalization Talents Program (XLYC2007060), and the Scientific Research Foundation of Educational Department of Liaoning Province (LJC202004).

References

1 (*a*) C. Han, X. Zhang, S. Huang, Y. Hu, Z. Yang, T. Li, Q. Li and J. Qian, *Adv. Sci.*, 2023, **10**, 2300797; (*b*) K. Wang, J. Zhang, Y. Hsu, H. Lin, Z. Han, J. Pang, Z. Yang, R. Liang, W. Shi and H. Zhou, *Chem. Rev.*, 2023, **123**(9), 5347–5420; (*c*) C. Yuan, D. Luo, L. Zhong, H. Deng, D. Liu, P. Xu and P. Dai, *Angew. Chem., Int. Ed.*, 2011, **50**, 3515–3519.

2 (*a*) Y. Tian, B. Chen, S. Zhang and Y. Zhang, *Chem. Eng. J.*, 2024, **479**, 147782; (*b*) P. Sudarsanam, H. Li and T. Sagar, *ACS Catal.*, 2020, **10**, 9555–9584; (*c*) Y. Zhong, Q. Deng, Q. Yao, C. Lu, P. Zhang, H. Li, J. Wang, Z. Zeng, J. Zou and S. Deng, *ACS Sustainable Chem. Eng.*, 2020, **8**, 7785–7794.

3 Z. Zhao, J. Yang, N. Xu, T. Nan, P. Wu, C. Wang, X. Wang, P. Bai, Z. Yan and S. Mintova, *Inorg. Chem. Front.*, 2023, **10**, 1574–1586.

4 X. Chen, D. Huang, L. He, L. Zhang, Y. Ren, X. Chen, B. Yue and H. He, *J. Phys. Chem. C*, 2021, **125**, 9330–9341.

5 (*a*) M. Tan, S. Tian, T. Zhang, K. Wang, L. Xiao, J. Liang, Q. Ma, G. Yang, N. Tsubaki and Y. Tan, *ACS Catal.*, 2021, **11**, 4633–4643; (*b*) B. Zhang, X. Bai, S. Wang, L. Li, X. Li, F. Fan, T. Wang, L. Zhang, X. Zhang, Y. Li, Y. Liu, J. Chen, F. Meng and Y. Fu, *ACS Appl. Mater. Interfaces*, 2021, **13**, 32175–32183; (*c*) X. Han, T. Zhang, M. Biset-Peiró, S. Zhao, S. Lopez, K. Daasbjerg, J. Morante, J. Li and J. Arbiol, *Small Struct.*, 2023, **4**, 2200388.

6 (*a*) Y. Zhao, T. Sun, W. Liao, Y. Wang, J. Yu, M. Zhang, Z. Yu, B. Yang, D. Gui, C. Zhu and J. Xu, *ACS Appl. Mater. Interfaces*, 2019, **11**, 22794–22800; (*b*) J. Wang, Y. Li, H. Li, Z. Cui, Y. Hou, W. Shi, K. Jiang, L. Qu and Y. Zhang, *J. Hazard. Mater.*, 2019, **379**, 120806; (*c*) H. Fujisaki, T. Ishizuka, H. Kotani and T. Kojima, *ACS Catal.*, 2024, **14**, 2609–2619.

7 (*a*) B. Snyder, A. Turkiewicz, H. Furukawa, M. Paley, E. Velasquez, M. Dods and J. Long, *Nature*, 2023, **613**, 287–291; (*b*) V. Guillerm and D. Maspoch, *J. Am. Chem. Soc.*, 2019, **141**, 16517–16538; (*c*) H. Jiang, S. Moosavi, J. Czaban-Jóźwiak, B. Torre, A. Shkurenko, Z. Ameur, J. Jia, N. Alsadun, O. Shekhah, E. Fabrizio, B. Smit and M. Eddaoudi, *Matter*, 2023, **6**, 285–295; (*d*) X. Xu, Q. Cui, H. Chen and N. Huang, *J. Am. Chem. Soc.*, 2023, **145**, 24202–24209; (*e*) X. Xu, X. Wu, K. Xu, H. Xu, H. Chen and N. Huang, *Nat. Commun.*, 2023, **14**, 3360; (*f*) L. Yang, P. Cai, L. Zhang, X. Xu, A. Yakovenko, Q. Wang, J. Pang, S. Yuan, X. Zou, N. Huang, Z. Huang and H. Zhou, *J. Am. Chem. Soc.*, 2021, **143**, 12129–12137.

8 (*a*) M. Ding, R. Flaig, H. Jiang and O. Yaghi, *Chem. Soc. Rev.*, 2019, **48**, 2783–2828; (*b*) L. Jiao and H. Jiang, *Chem*, 2019, **5**, 786–804.

9 M. Nandasiri, S. Jambovane, B. McGrail, H. Schaef and S. Nune, *Coord. Chem. Rev.*, 2016, **311**, 38–52.

10 X. Meng, H. Wang, S. Song and H. Zhang, *Chem. Soc. Rev.*, 2017, **46**, 464–480.

11 (*a*) W. Zhang, Y. Hu, J. Ge, H. Jiang and S. Yu, *J. Am. Chem. Soc.*, 2014, **136**, 16978–16981; (*b*) S. Yuan, L. Feng, K. Wang, J. Pang, M. Bosch, C. Lollar, Y. Sun, J. Qin, X. Yang, P. Zhang, Q. Wang, L. Zou, Y. Zhang, L. Zhang, Y. Fang, J. Li and H. Zhou, *Adv. Mater.*, 2018, **30**, 1704303; (*c*) A. Dhakshinamoorthy, M. Alvaro and H. Garcia, *Adv. Synth. Catal.*, 2010, **352**, 3022–3030; (*d*) M. Xu, D. Li, K. Sun, L. Jiao, C. Xie, C. Ding and H. Jiang, *Angew. Chem., Int. Ed.*, 2021, **60**, 16372–16376.

12 (*a*) G. Huang, Q. Yang, Q. Xu, S. Yu and H. Jiang, *Angew. Chem., Int. Ed.*, 2016, **55**, 7379–7383; (*b*) H. Lee, C. Koh, Y. Lee, C. Liu, I. Phang, X. Han, C. Tsung and X. Ling, *Sci. Adv.*, 2018, **4**, eaar3208; (*c*) L. Xie, M. Xu, X. Liu, M. Zhao and J. Li, *Sci. Adv.*, 2020, **7**, 1901758.

13 (*a*) H. Zhou and S. Kitagawa, *Chem. Soc. Rev.*, 2014, **43**, 5415–5418; (*b*) J. Nguyen and S. Cohen, *J. Am. Chem. Soc.*, 2010, **132**, 4560–4561; (*c*) C. Serre, *Angew. Chem., Int. Ed.*, 2012, **51**, 6048–6050.

14 (*a*) Y. Sun, Q. Sun, H. Huang, B. Aguila, Z. Niu, J. Perman and S. Ma, *J. Mater. Chem. A*, 2017, **5**, 18770–18776; (*b*) M. Gao, S. Zhao, Z. Chen, L. Liu and Z. Han, *Inorg. Chem.*, 2019, **58**, 2261–2264.

15 (*a*) L. Wang, M. Fang, J. Liu, J. He, J. Li and J. Lei, *ACS Appl. Mater. Interfaces*, 2015, **7**, 24082–24093; (*b*) U. Tran, K. Le and N. Phan, *ACS Catal.*, 2011, **1**, 120–127; (*c*) K. Jayaramulu, K. Datta, C. Rösler, M. Petr, M. Otyepka, R. Zboril and R. Fischer, *Angew. Chem., Int. Ed.*, 2016, **55**, 1178–1182; (*d*) A. Huang, Q. Liu, N. Wang, Y. Zhu and J. Caro, *J. Am. Chem. Soc.*, 2014, **136**, 14686–14689.

16 W. Chi, S. Kim, S. Lee, Y. Bae and J. Kim, *ChemSusChem*, 2015, **8**, 650–658.

17 (*a*) S. Chen, X. Li, E. Dong, H. Lv, X. Yang, R. Liu and B. Liu, *J. Phys. Chem. C*, 2019, **123**, 29693–29707; (*b*) A. Awadallah-F, F. Hillman, S. Al-Muhtaseb and H. Jeong, *J. Mater. Sci.*, 2019, **54**, 5513–5527.

18 S. Oishi, K. Oi, J. Kuwabara, R. Omoda, Y. Aihara, T. Fukuda, T. Takahashi, J. Choi, M. Watanabe and T. Kanbara, *ACS Appl. Polym. Mater.*, 2019, **1**, 1195–1202.

19 (*a*) S. Venna, J. Jasinski and M. Carreon, *J. Am. Chem. Soc.*, 2010, **132**, 18030–18033; (*b*) S. Venna and M. Carreon, *J. Am. Chem. Soc.*, 2010, **132**, 76–78.

20 D. Mullangi, S. Shalini, S. Nandi, B. Choksi and R. Vaidhyanathan, *J. Mater. Chem. A*, 2017, **5**, 8376–8334.

21 (*a*) K. Wenderich and G. Mul, *Chem. Rev.*, 2016, **116**, 14587–14619; (*b*) Q. Yang, Q. Xu and H. Jiang, *Chem. Soc. Rev.*, 2017, **46**, 4774–4808; (*c*) J. Bi, J. Chen, Y. Dong, W. Guo, D. Zhu and T. Li, *J. Polym. Sci., Part A: Polym. Chem.*, 2018, **56**, 2344–2353.

22 J. Ma and S. Kass, *J. Org. Chem.*, 2019, **84**, 11125–11134.

23 (*a*) R. Kusurkar, N. Alkobati, A. Gokule and V. Puranik, *Tetrahedron*, 2008, **64**, 1654–1662; (*b*) A. Bahuguna, A. Kumar, S. Kumar, T. Chhabra and V. Krishnan, *ChemCatChem*, 2018, **10**, 3121–3132.

24 (*a*) C. McGuirk, M. Katz, C. Stern, A. Sarjeant, J. Hupp, O. Farha and C. Mirkin, *J. Am. Chem. Soc.*, 2015, **137**, 919–925; (*b*) X. Dong, T. Liu, Y. Hu, X. Liu and C. Che, *Chem. Commun.*, 2013, **49**, 7681–7683; (*c*) C. Zhu, Q. Mao, D. Li, C. Li, Y. Zhou, X. Wu, Y. Luo and Y. Li, *Catal. Commun.*, 2018, **104**, 123–127; (*d*) X. Zhang, Z. Zhang, J. Boissonnault and S. Cohen, *Chem. Commun.*, 2016, **52**, 8585–8588; (*e*) P. Rao and S. Mandal, *ChemCatChem*, 2017, **9**, 1172–1176; (*f*) D. Markad and S. Mandal, *ACS Catal.*, 2019, **9**, 3165–3173; (*g*) A. Nagaraj and D. Amarajothi, *J. Colloid Interface Sci.*, 2017, **494**, 282–289.

25 (*a*) C. Van Goethem, M. Mertens, F. Cirujano, J. Seo, D. De Vos and I. Vankelecom, *Chem. Commun.*, 2018, **54**, 7370–7373; (*b*) Y. Rao, F. Ni, Y. Sun, B. Zhu, Z. Zhou and Z. Yao, *Sep. Purif. Technol.*, 2020, **230**, 115844; (*c*) X. Jiang, H. Chen, L. Liu, L. Qiu and X. Jiang, *J. Alloys Compd.*, 2015, **646**, 1075–1082.